


## Article

# A New Climatology of Vegetation and Land Cover Information for South America

Laurizio Emanuel Ribeiro Alves <sup>1,\*</sup> , Luis Gustavo Gonçalves de Gonçalves <sup>1,2</sup> , Álvaro Vasconcellos Araújo de Ávila <sup>1</sup>, Giovana Deponte Galetti <sup>1</sup>, Bianca Buss Maske <sup>1</sup>, Giuliano Carlos do Nascimento <sup>3</sup> and Washington Luiz Félix Correia Filho <sup>4</sup> 

<sup>1</sup> Centro de Previsão de Tempo e Estudos Climáticos (CPTEC), Instituto Nacional de Pesquisas Espaciais (INPE), Cachoeira Paulista 12630-000, Brazil; luis.goncalves@cmcc.it (L.G.G.d.G.); giovana.galetti@inpe.br (G.D.G.)

<sup>2</sup> Fondazione Centro Euro-Mediterraneo sui Cambiamenti Climatici (CMCC), 73100 Lecce, Italy

<sup>3</sup> Centro de Monitoramento de Alerta e Alarme da Defesa Civil (CEMADEC), Defesa Civil de Salvador (CODESAL), Salvador 40301-110, Brazil

<sup>4</sup> Programa de Pós-Graduação em Ambientometria, Universidade Federal do Rio Grande (FURG), Rio Grande 96203-900, Brazil; washington.correia@furg.br

\* Correspondence: laurizio.alves@inpe.br; Tel.: +55-82-99404-0036

**Abstract:** Accurate information on vegetation and land cover is crucial for numerical forecasting models in South America. This data aids in generating more realistic forecasts, serving as a tool for decision-making to reduce environmental impacts. Regular updates are necessary to ensure the data remains representative of local conditions. In this study, we assessed the suitability of ‘Catchment Land Surface Models-Fortuna 2.5’ (CLSM), Noah, and Weather Research and Forecasting (WRF) for the region. The evaluation revealed significant changes in the distribution of land cover classes. Consequently, it is crucial to adjust this parameter during model initialization. The new land cover classifications demonstrated an overall accuracy greater than 80%, providing an improved alternative. Concerning vegetation information, outdated climatic series for Leaf Area Index (LAI) and Greenness Vegetation Fraction (GVF) were observed, with notable differences between series, especially for LAI. While some land covers exhibited good performance for GVF, the Forest class showed limitations. In conclusion, updating this information in models across South America is essential to minimize errors and enhance forecast accuracy.

**Keywords:** land parameters; land input; climatology



**Citation:** Alves, L.E.R.; Gonçalves, L.G.G.d.; Ávila, Á.V.A.d.; Galetti, G.D.; Maske, B.B.; Nascimento, G.C.d.; Correia Filho, W.L.F. A New Climatology of Vegetation and Land Cover Information for South America. *Sustainability* **2024**, *16*, 2606. <https://doi.org/10.3390/su16072606>

Academic Editor: Hariklia D. Skilodimou

Received: 6 January 2024

Revised: 5 February 2024

Accepted: 7 February 2024

Published: 22 March 2024



**Copyright:** © 2024 by the authors. Licensee MDPI, Basel, Switzerland. This article is an open access article distributed under the terms and conditions of the Creative Commons Attribution (CC BY) license (<https://creativecommons.org/licenses/by/4.0/>).

## 1. Introduction

South America, situated in the equatorial and tropical zones, has a rich and heterogeneous flora. SA poses challenges in accurately depicting Earth’s surface characteristics, because large agricultural areas mix with forests and savannas, complicating the region’s land surface characterization. This complexity is generally poorly represented in land cover (LC) maps and global vegetation information [1–3]. Additionally, the expansion of agricultural frontiers in the central region of SA, along with documented cases of deforestation and wildfires [4–6], makes it even more challenging to accurately represent this information. These events occur regularly every year, contributing to the land surface degradation in SA over the years [7,8].

The South American Land Data Assimilation System (SALDAS) is a system that was developed for SA to help understand the conditions of the Earth’s surface and improve the process of initializing regional atmospheric models. This system uses recent spatial observation data acquired from a network of ground observations [9–11]. The terrestrial data system includes surface variables such as soil moisture, vegetation (Leaf Area Index—LAI, a metric quantifying the green leaf area relative to the ground area and serving as a crucial indicator in characterizing the canopy structure in forest ecosystems [12]; and Greenness Vegetation Fraction—GVF, representing the green vegetation fraction covering a unit ground area as seen from the nadir direction) [13], LC, albedo, and topography.

This study will analyze the effectiveness of three different surface models used in the operational models of SA: Noah, Catchment LSM-Fortuna 2.5—CLSM, and Weather Research and Forecasting—WRF [14–16]. The evaluation will use its surface parameters as LAI (representing vertical vegetation density characteristics), GVF (illustrating horizontal vegetation density), and LC (identifying prevalent plant types within a numerical model grid cell, used to simulate additional specific surface parameters) [17,18].

Surface parameters are crucial in simulating surface fluxes (energy, water, and carbon) and are employed by various surface, weather, and climate models [17,19–23]. Therefore, it is expected that the information from LAI, GVF, and LC will exhibit a high correlation with actual observed data, both temporally and spatially, contributing to an optimal initialization for the operational models of SA. This update will contribute to the short-term simulations for operational environments related to changes in the water cycle [24], predictions of adverse events that cause landslides [25], or midterms in the prediction of seasonal forecasts of heatwaves [26] and forecasts for climate change [27].

Furthermore, surface information from operational models needs periodic updates (every 5 to 10 years) to prevent the information from becoming too outdated [28]. In this perspective, a new LC climatology for SA will be developed based on products from the European Space Agency Climate Change Initiative (ESACCI), updated annually globally [1]. The new LC will be compared to input information from land and atmospheric models (Noah, CLSM, and WRF). Furthermore, a new LAI and GVF climatology will be created based on the Global Land Surface Satellite (GLASS) products. GLASS was chosen for its ability to mitigate cloud contamination effects in data from the Moderate-Resolution Imaging Spectroradiometer (MODIS) using the General Regression Neural Networks (GRNNs) method, making it a more refined product for surface assessments [29–31]. This new climatology will be compared to the input information of numerical models in SA.

Therefore, the following questions are raised: (1) is the LC used in the LSMs for SA significantly outdated compared to the distribution of land cover classes presented by new LC products based on ESACCI data? (2) Is the input information for numerical models (NM) regarding LAI and GVF consistent with the new GLASS climatology?

Given the above, this study aims to assess the surface input information (LAI, GVF, and LC) used by operational/research models and develop new climatology based on this information to improve the initial conditions of SA models.

## 2. Materials and Methods

The flowchart of the methodology steps in this study is presented in Figure 1, which is detailed in the following subtopics.

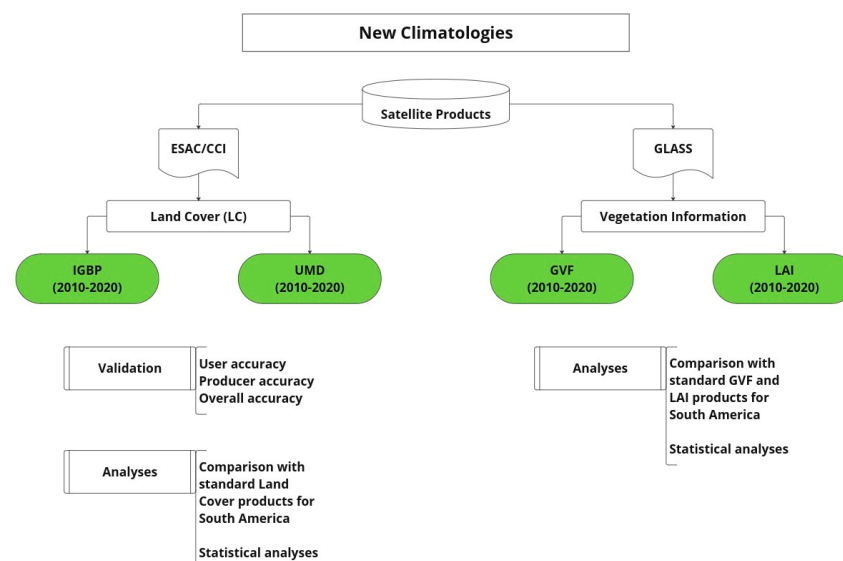


**Figure 1.** Flowchart of the methodology of this work.

### 2.1. Land Cover Products

For land cover (LC), remote sensing products were obtained from ESACCI (ESACCI-LC), sourced from the Copernicus Climate Data Store (CDS) were accessed on 18 February 2023, available at <https://cds.climate.copernicus.eu/cdsapp!/dataset/satellite-land-cover?%20tab=form>. The land use and land cover maps have a spatial resolution of 300 m worldwide, describing the Earth’s surface in 22 classes and 14 subclasses (36 LC classifications) based on the United Nations Food and Agriculture Organization’s Land Cover Classification System (UN FAO—LCCS). Additionally, the maps are provided in NetCDF (.nc) format with an annual temporal resolution from 1992 to the present [32].

The selection of the ESACCI-LC product is due to its high accuracy in several land cover types, including evergreen broadleaf forests, urban areas, bare soil, permanent water bodies, and permanent snow/ice, with accuracies exceeding 80%. It is worth noting that agricultural areas exhibit high precision (above 83%), even in their high heterogeneity, which is crucial for agricultural planning and food security [33]. These areas are particularly relevant in SA, where extensive agricultural areas and heterogeneous land cover are prominent.

ESACCI-LC products were downloaded from 2010 to 2020 for this study, considering the most recent land use and land cover availability information. A climatology map was generated using the LC information from this period. The map was reprojected to the Coordinate Reference System (CRS) 4326—World Geodetic System 1984 (WGS84)—Geographic. Additionally, it was resized to a resolution of  $0.01^\circ$  (~1 km) using the “Mode” method, which employs the most frequent value of LC information within the new pixel area. In other words, the most frequently occurring class in a given area will become the class for the new pixel area, as illustrated in Figure 2. Note in this figure that green pixels have a higher frequency in the new pixel area and, because of this, the resampled pixel will only be classified as green.

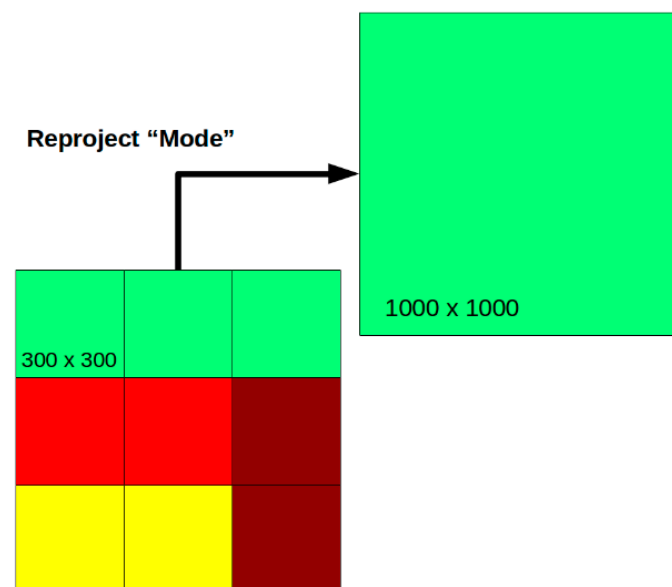


**Figure 2.** Reprojection of LC pixel area.

Furthermore, the new LC map was reclassified into the Modified International Geosphere-Biosphere Programme (IGBP—20 classes) [34] and the University of Maryland (UMD—13 classes) [35]. For this purpose, the ‘Reclassify by table’ extension tool, available in QGIS 3.16 software, was used. This tool established correspondences between the map classified according to the UN FAO and the mentioned classes, as shown in Table 1.

**Table 1.** Conversion of ESACCI-LC classes to the new classifications.

ID. ESACCI Classification	ID. UMD Classification	ID. IGBP Classification
10. Cropland, Rainfed	11. Cropland	12. Croplands
11. Cropland, Rainfed, Herbaceous Cover	11. Cropland	12. Croplands
12. Cropland, Rainfed, Tree or Shrub Cover	8. Closed Bushlands or Shrublands	6. Closed Shrublands
20. Cropland, Irrigated or Post-Flooding	11. Cropland	12. Croplands
30. Mosaic Cropland (>50%)/Natural Vegetation (Tree, Shrub, Herbaceous Cover) (<50%)	7. Wooded Grasslands/Shrublands	14. Cropland/Natural Vegetation
40. Mosaic Natural Vegetation (Tree, Shrub, Herbaceous Cover) (>50%)/Cropland (<50%)	11. Cropland	14. Cropland/Natural Vegetation
50. Tree Cover, Broadleaved, Evergreen, Closed to Open (>15%)	2. Evergreen Broadleaf Forest	2. Evergreen Broadleaf Forest
60. Tree Cover, Broadleaved, Deciduous, Closed to Open (>15%)	4. Deciduous Broadleaf Forest	4. Deciduous Broadleaf Forest
61. Tree Cover, Broadleaved, Deciduous, Closed (>40%)	6. Woodlands	4. Deciduous Broadleaf Forest
62. Tree Cover, Broadleaved, Deciduous, Open (15–40%)	7. Wooded Grasslands/Shrublands	8. Woody Savannas
70. Tree Cover, Needleleaved, Evergreen, Closed To Open (>15%)	1. Evergreen Needleleaf Forest	1. Evergreen Needleleaf Forest
71. Tree Cover, Needleleaved, Evergreen, Closed (>40%)	2. Evergreen Needleleaf Forest	1. Evergreen Needleleaf Forest
72. Tree Cover, Needleleaved, Evergreen, Open (15–40%)	2. Evergreen Needleleaf Forest	1. Evergreen Needleleaf Forest
80. Tree Cover, Needleleaved, Deciduous, Closed to Open (>15%)	3. Deciduous Needleleaf Forest	3. Deciduous Needleleaf Forest
81. Tree Cover, Needleleaved, Deciduous, Closed (>40%)	3. Deciduous Needleleaf Forest	3. Deciduous Needleleaf Forest
82. Tree Cover, Needleleaved, Deciduous, Open (15–40%)	3. Deciduous Needleleaf Forest	3. Deciduous Needleleaf Forest
90. Tree Cover, Mixed Leaf Type (Broadleaved and Needleleaved)	5. Mixed Forest	5. Mixed Forest
100. Mosaic Tree and Shrub (>50%)/Herbaceous Cover (<50%)	7. Wooded Grasslands/Shrublands	8. Woody Savannas
110. Mosaic Herbaceous Cover (>50%)/Tree and Shrub (<50%)	7. Wooded Grasslands/Shrublands	9. Savannas
120. Shrubland	7. Wooded Grasslands/Shrublands	9. Savannas
121. Evergreen Shrubland	8. Closed Bushlands or Shrublands	6. Closed Shrublands
122. Deciduous Shrubland	7. Wooded Grasslands/Shrublands	9. Savannas
130. Grassland	10. Grassland	10. Grassland
140. Lichens and Mosses	10. Grassland	10. Grassland
150. Sparse Vegetation (Tree, Shrub, Herbaceous Cover) (<15%)	9. Open Shrubland	7. Open Shrublands
151. Sparse Tree (<15%)	9. Open Shrubland	7. Open Shrublands
152. Sparse Shrub (<15%)	9. Open Shrubland	7. Open Shrublands
153. Sparse Herbaceous Cover (<15%)	9. Open Shrubland	7. Open Shrublands
160. Tree Cover, Flooded, Fresh or Brackish Water	8. Closed Bushlands or Shrublands	11. Permanent wetlands
170. Tree Cover, Flooded, Saline Water	8. Closed Bushlands or Shrublands	11. Permanent wetlands
180. Shrub or Herbaceous Cover, Flooded, Fresh/Saline/Brackish Water	6. Woodlands	11. Permanent wetlands
190. Urban Areas	13. Urban and Built-Up	13. Urban and Built-Up
200. Bare Areas	12. Bare Ground	16. Barren or Sparsely Vegetated
201. Consolidated Bare Areas	12. Bare Ground	16. Barren or Sparsely Vegetated
202. Unconsolidated Bare Areas	12. Bare Ground	16. Barren or Sparsely Vegetated
210. Water Bodies	0. Water bodies	17. Water
220. Permanent Snow and Ice	12. Barren	15. Permanent and Snow and Ice

The QGIS 3.16 used the AcATaMa plugin [36] to evaluate the accuracy of land cover reclassification. This plugin is a crucial step in determining how well the representation of land cover matches the actual land cover on the ground [37]. Sampling points were created

to validate the reclassification process using ‘Stratified Random Sampling’. The plugin determined the required samples for each class with a standard deviation of 0.005 [38,39]. The plugin also automatically generated a distribution of points.

Each point was assigned a class through a supervised identification process. It is worth noting that the samples were taken from satellite images with higher spatial resolution, such as Google Satellite and Bing Virtual Earth, as well as GLASS LAI and GVF products. After choosing the points, accuracy was calculated using the formulas mentioned in [38,39]. The results are presented in tables of the Error Matrix, providing (i) the user’s accuracy, which is an estimation of the fractions of pixels in the mapping for each category correctly classified, associated with the commission error, which happens when a category is incorrectly assigned to a pixel. Thus, user accuracy is related to the reliability of each mapped class. (ii) The producer’s accuracy, the sample reliability of pixels for each class correctly assigned by the classifiers, and with omission error, which occurs when a pixel is not correctly mapped to its class.

Hence, producer accuracy is linked to the classifier’s sensitivity to correctly distinguish mapping classes. (iii) Overall accuracy is the overall proportion of correct classifications for all mapping classes. A comparative assessment was conducted to investigate differences in land use and land cover between the input LC of the models and the products from the new LC climatology by ESACCI, reclassified into UMD and IGBP classes.

## 2.2. Vegetation Products

The images of remote sensing products come from the Moderate-Resolution Imaging Spectroradiometer (MODIS) sensor reprocessed by the University of Maryland for the Global Land Surface Satellite (GLASS) project. This project reduces the effects of cloud contamination in MODIS products through the General Regression Neural Networks (GRNNs) method based on satellite images with higher spatial resolution, such as Landsat and SPOT [29–31,40,41].

The GLASS products are available at the University of Maryland image collection on the website <http://www.glass.umd.edu/Download.html> and were accessed on 12 March 2023. The acquisition area of the products covers the entire globe. Furthermore, the data period spans from January 2010 to December 2020, with an 8-day temporal frequency, acquired in Hierarchical Data Format (HDF), and a spatial resolution of 0.05°. The acquired products include GLASS LAI and GLASS Fractional Vegetation Cover (FVC). In this study, it will be referred to as GLASS GVF, as the calculation formula for FVC is similar to GVF [21,41], given by Equation (1):

$$GVF = FVC = \frac{NDVI - NDVI_S}{NDVI_V - NDVI_S} \quad (1)$$

where  $NDVI$  is the Normalized Difference Vegetation Index and  $NDVI_S$  and  $NDVI_V$  are the  $NDVI$  for exposed soil and soil with higher vegetation cover, respectively.

Finally, a comparative assessment was conducted for the standard LAI and GVF in numerical models of SA, based on [42,43], respectively, against GLASS products to examine differences in vegetation characteristics’ behavior. For this purpose, point values were extracted for four land classes:

- (1) Forest (for IGBP and UMD, representing the Evergreen Needleleaf Forest class);
- (2) Savanna (for IGBP, this class represents Savanna, while for UMD, it is Wooded Grassland/Shrublands);
- (3) Agriculture (for IGBP and UMD, representing the Cropland class);
- (4) Grass (for IGBP and UMD, representing the Grassland class).

Table 2 presents the coordinates of the land classes.

**Table 2.** Coordinates of land classes.

Land Class	Latitude	Longitude
Forest	−2.60°	−60.20°
Savanna	−15.93°	−47.72°
Cropland	−30.27°	−53.13°
Grass	−31.72°	−53.53°

The statistical metrics used to assess the behavioral pattern of vegetation include Pearson correlation coefficient ( $r$ ), determination coefficient ( $R^2$ ), statistical bias, Willmott's index of concordance ( $d$ ), and confidence coefficient ( $c$ ). Please refer to the sources [44–46] for more details. The following Tables 3 and 4 present the criteria for assessing  $r$  and  $c$ .

**Table 3.** Description of values of Pearson correlation ( $r$ ).

Correlation Coefficient “ $r$ ”	Description
0.00 to 0.19	Very weak correlation
0.20 to 0.39	Weak correlation
0.40 to 0.69	Moderate correlation
0.70 to 0.89	Strong correlation
0.90 to 1.00	Very strong correlation

Font: [46].

**Table 4.** Performance of the confidence index ( $c$ ).

Confidence Index “ $c$ ”	Performance
>0.85	Excellent
0.76 to 0.85	Very good
0.66 to 0.75	Good
0.61 to 0.65	Average
0.51 to 0.60	Poor
0.41 to 0.50	Bad
≤0.40	Terrible

Font: [44].

Moreover, to evaluate the variability of vegetation information, we utilized the 2000–2022 rainfall climatology from the Multi-Source Weighted-Ensemble Precipitation (MERGE) [47]. Monthly rainfall accumulations served as the basis for this assessment. Access to these data is provided on the following website: <http://ftp.cptec.inpe.br/modelos/tempo/MERGE/GPM/CLIMATOLOGY/> and were accessed on 22 March 2023.

### 3. Results and Discussion

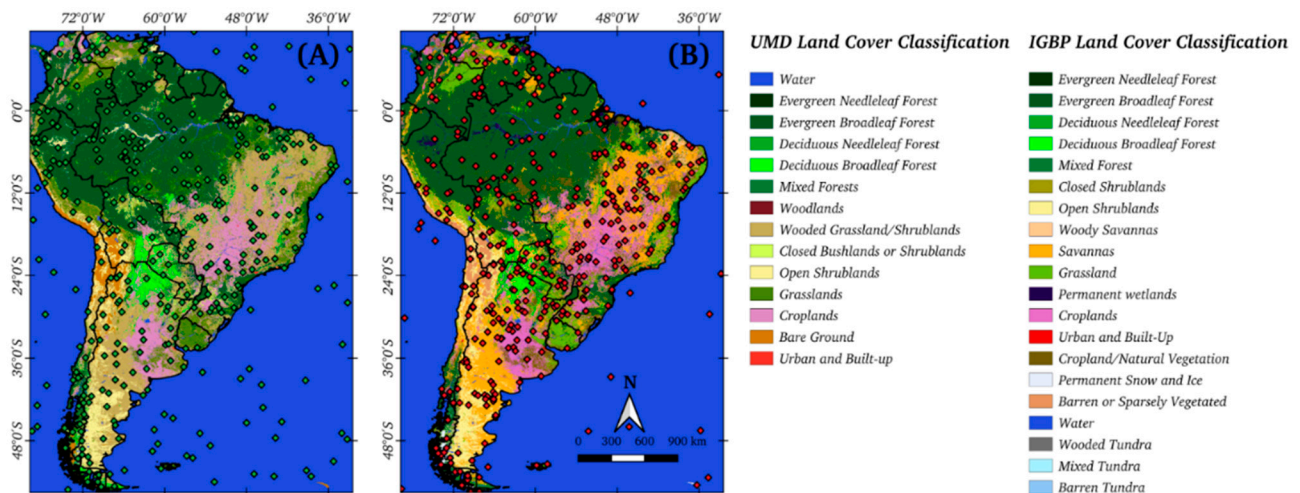
#### 3.1. New Land Cover Climatology

Figure 3 exhibits the new land cover maps based on the 2010–2020 climatology of the ESACCI product, reclassified for the IGBP classifications (Figure 3A) and UMD classifications (Figure 3B), respectively. Additionally, validation control points used in constructing the error matrix for various land cover classes are highlighted, totaling more than 400 points per thematic map.

Confusion/error matrices and their producer and user accuracies for IGBP and UMD classes are displayed in Tables 5 and 6. These matrices are derived from the new ESACCI LC data spanning 2010–2020. This analysis is the primary method for evaluating mapping quality, offering an overall accuracy rate tied to Global Accuracy. It also provides accuracy and error rate estimates for each mapped class.

In Table 5, the confusion matrix analysis reveals the most significant misclassification error for IGBP in the Cropland/Natural Vegetation class, where confusion occurs with Croplands and Savannas' classes. This confusion is easily explained when examining the Croplands class, as they are similar classes, and the coarser resolution of 0.01°

may contribute to lower mapping precision in these circumstances. As for the Savannas class, representing the Brazilian Cerrado and Caatinga, classification confusion may be attributed to agricultural boundaries, deforestation, and variations in vegetation vigor due to rainfall [48,49].



**Figure 3.** Land cover (LC) map for UMD (A); and IGBP (B) classifications for SA, as well as validation sampling points for UMD (green dots) and IGBP (red dots).

The changes in land use and land cover between 2009 and 2018 are linked to the deforestation of the Cerrado and its replacement by agricultural areas [50]. This modification in land cover influences climatology because abrupt changes in land cover result in greater variability in the affected region's coverage type. In this sense, updating this information is essential to ensure that the initial conditions of numerical models do not become outdated.

According to Table 5, the Cropland/Natural Vegetation class shows a user accuracy of 56.0% ( $\pm 10.1\%$ ) with a high commission error, indicating unreliable mapping. Similarly, the Savannas class has a user accuracy of 57.4% ( $\pm 6.8\%$ ). In contrast, the Cropland class demonstrates a user accuracy of 75.0% ( $\pm 6.6\%$ ), considered reasonable for large, mapped areas.

Regarding producer accuracy, the values for the Cropland/Natural Vegetation, Savannas, and Cropland classes are 43.1% ( $\pm 7.3\%$ ), 92.15% ( $\pm 3.3\%$ ), and 72.64% ( $\pm 6.1\%$ ), respectively (Table 5). Notably, only the Cropland/Natural Vegetation class exhibits a high omission error associated with incorrectly assigning the class to the pixel. In contrast, the Savannas and Cropland classes have low omission errors.

Table 5 indicates that more homogeneous land covers, such as Evergreen Broadleaf Forest, Permanent Snow and Ice, Barren or Sparsely Vegetated, and Water classes, boast user accuracy exceeding 80%, resulting in low commission errors. For omission errors associated with producer accuracy, these classes have the following values: 96.17% ( $\pm 1.66\%$ ), 45.43% ( $\pm 17.93\%$ ), 55.95% ( $\pm 9.66\%$ ), and 100% (0), respectively. From this perspective, the Permanent Snow and Ice, Barren, or Sparsely Vegetated classes demonstrate low reliability, while the Evergreen Broadleaf Forest and Water classes exhibit high producer accuracy.

Classes like Wooded Tundra, Mixed Tundra, and Barren Tundra, with smaller coverage areas over SA, show low reliability in samples since their coverage is less than 900 km<sup>2</sup> (Table 5). Consequently, only a few sampling points (7) were generated for these Tundra classes. In the case of the Urban and Built-up class, there is a producer accuracy of only 35.5% and a user accuracy of 90%, indicating high omission and low commission errors.

**Table 5.** Confusion matrix and user (UA) and producer (PA) accuracies of IGBP land cover from ESACCI 2010–2020 climatology over SA.

Land Cover Class Description	1	2	3	4	5	6	7	8	9	10	11	12	13	14	15	16	17	18	19	20	Total	UA * (%)
1. Evergreen Needleleaf Forest	7	0	0	0	0	0	0	0	0	0	0	2	0	1	0	0	0	0	0	0	10	70.0
2. Evergreen Broadleaf Forest	0	55	0	0	1	2	0	0	0	1	3	0	0	1	0	0	0	0	0	0	64	85.0
3. Deciduous Needleleaf Forest	0	3	4	0	0	0	1	0	0	0	1	0	0	1	0	0	0	0	0	0	10	40.0
4. Deciduous Broadleaf Forest	0	0	0	9	0	2	0	0	1	1	0	0	0	0	0	0	0	0	0	0	13	69.2
5. Mixed Forest	0	0	1	0	11	0	0	0	1	0	0	0	0	0	0	0	0	0	0	1	14	78.6
6. Closed Shrublands	0	0	0	0	0	10	0	0	0	2	0	0	1	2	0	0	0	0	0	0	15	66.7
7. Open Shrublands	0	1	0	0	0	0	18	0	0	0	0	0	0	1	0	4	0	0	0	0	24	75.0
8. Woody Savannas	0	0	0	0	0	0	0	5	4	0	0	1	0	1	0	0	0	0	0	0	11	45.5
9. Savannas	0	0	0	0	1	0	8	1	31	2	0	4	0	6	0	1	0	0	0	0	54	57.4
10. Grassland	0	0	0	0	2	0	5	0	0	18	1	3	1	1	1	1	0	0	0	0	33	54.5
11. Permanent Wetlands	0	2	0	0	0	0	0	0	0	0	9	0	0	0	0	0	0	0	0	0	11	81.8
12. Croplands	0	0	0	0	0	0	1	0	0	4	0	33	0	6	0	0	0	0	0	0	44	75.0
13. Urban and Built-Up	0	0	0	0	0	0	0	0	0	0	0	1	9	0	0	0	0	0	0	0	10	90.0
14. Cropland/Natural Vegetation	0	3	0	0	1	0	0	0	1	3	0	3	1	14	0	0	0	0	0	0	25	56.0
15. Permanent Snow and Ice	0	0	0	0	0	0	0	0	0	0	0	0	0	0	9	1	0	0	0	0	11	81.8
16. Barren or Sparsely Vegetation	0	0	0	0	0	0	0	0	0	0	0	1	0	0	1	13	0	0	0	0	15	86.7
17. Water	0	0	0	0	0	0	0	0	0	0	0	0	0	0	0	0	20	0	0	0	20	100.0
18. Wooded Tundra	0	0	0	0	1	0	1	0	0	2	0	0	0	3	0	0	0	3	0	0	10	30.0
19. Mixed Tundra	0	0	0	0	1	0	0	1	0	0	0	4	0	2	0	0	0	0	2	0	10	20.0
20. Barren Tundra	1	0	0	0	0	0	1	0	0	1	0	6	0	1	0	0	0	0	0	0	10	0.0
Total	8	64	5	9	18	13	37	7	38	34	14	56	11	40	11	20	20	4	2	1	414	
PA **	96.9	96.2	90.4	100.0	49.9	64.1	47.3	52.5	92.2	58.3	26.2	72.6	35.5	43.1	45.4	55.9	100.0	1.8	100.0	100.0		

\* UA—User's Accuracy. \*\* Producer's Accuracy.



**Table 6.** Confusion matrix and user (UA) and producer (PA) accuracies of UMD land cover from ESACCI 2010–2020 climatology over SA.

Land Cover Class Description	1	2	3	4	5	6	7	8	9	10	11	12	13	Total	UA * (%)
1. Evergreen Needleleaf Forest	3	1	0	0	0	0	0	0	0	1	0	0	0	5	60.0
2. Evergreen Broadleaf Forest	0	84	0	0	2	0	0	0	0	0	4	0	0	90	93.3
3. Deciduous Needleleaf Forest	0	2	4	0	0	0	0	0	1	0	0	0	0	10	40.0
4. Deciduous Broadleaf Forest	0	0	0	10	0	0	0	2	1	1	0	1	0	15	66.7
5. Mixed Forest	0	0	1	0	9	0	0	0	1	0	0	0	0	10	90.0
6. Woodlands	0	0	0	0	0	0	0	0	0	0	0	0	0	0	0.0
7. Wooded Grassland/Shrublands	0	1	0	0	1	0	35	3	6	4	5	2	0	57	61.4
8. Closed Bushlands or Shrublands	0	0	0	0	0	0	0	13	1	1	0	0	0	15	86.7
9. Open Shrublands	0	1	0	0	0	0	1	0	15	0	0	3	0	20	75.0
10. Grassland	0	1	0	0	1	0	0	2	0	22	3	1	0	30	73.3
11. Croplands	0	0	0	0	0	0	0	0	0	2	27	0	0	29	93.1
12. Bare Ground	0	0	0	0	0	0	0	0	5	0	0	9	1	15	60.0
13. Urban and Built-Up	0	0	0	0	0	0	0	0	0	0	1	0	14	15	93.3
Total	3	88	5	10	13	0	36	20	29	31	40	16	15	301	
PA **	100.0	95.5	90.4	100.0	69.2	0.0	97.2	65.0	51.7	71.0	67.5	56.3	93.3		

\* UA—User’s Accuracy. \*\* Producer’s Accuracy.

The ESACCI 2010–2020 LC climatology achieved an overall accuracy of 89.83% ( $\pm 0.94\%$ ) over SA, surpassing the global accuracy of ESACCI (above 80%) [1,33]. This difference is due to the coarser resolution ( $0.01^\circ$ ) of the new LC climatology. The results highlight the new LC climatology’s high applicability and precision in defining LC classes.

Table 6 displays the error matrix for the UMD classification based on the ESACCI 2010–2020 LC climatology. The Open Shrubland class shows the highest omission error (producer accuracy), signifying misclassification and confusion in land cover. This class is often mistaken for Wooded Grassland/Shrubland due to similar characteristics, as observed in Figure 4, with a user accuracy of 75.0% ( $\pm 9.93\%$ ), indicating an acceptable commission error.

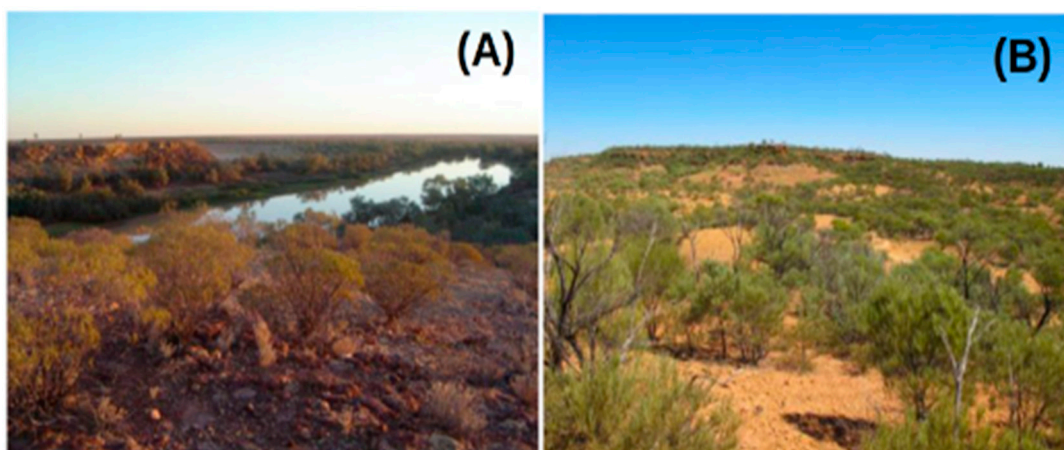


**Figure 4.** Classes of Open Shrublands (A); and Wooded Grassland/Shrublands (B).

Table 6 reveals that the Evergreen Needle Forest and Broadleaf Deciduous Forest classes achieve perfect producer accuracy (100.0%), correctly assigned at all control points. However, user accuracy reflects the reliability of each mapped class, which shows median values of 60.0% ( $\pm 24.5\%$ ) and 66.7% ( $\pm 12.6\%$ ). Notably, only the Evergreen Broadleaf Forest class surpasses 90.0% ( $\pm 2.4\%$ ) accuracy for both producer and user accuracy, making it the best-mapped class. For other classes, accuracy values, both for the user and the producer, hover around or fall below 80%.

The overall accuracy for the ESACCI-LC 2010–2020 climatology for UMD was 80.07% ( $\pm 2.31\%$ ), based on samples over SA (Table 6). This value is very close to the global

mapping of ESACCI, which reported a global accuracy slightly above 80% [1,33]. From these results, it is evident that the new LC climatology for 2010–2020 is highly applicable to the study region, demonstrating high precision in defining land use and land cover classes.

### 3.2. Land Cover Assessment over SA

Initially, the default LC maps of the numerical models in SA classified by IGBP [34] and UMD [35] were spatially compared to the new LC maps based on ESACCI. Figures 5 and 6 depict the LC maps for the two LSM classifications.

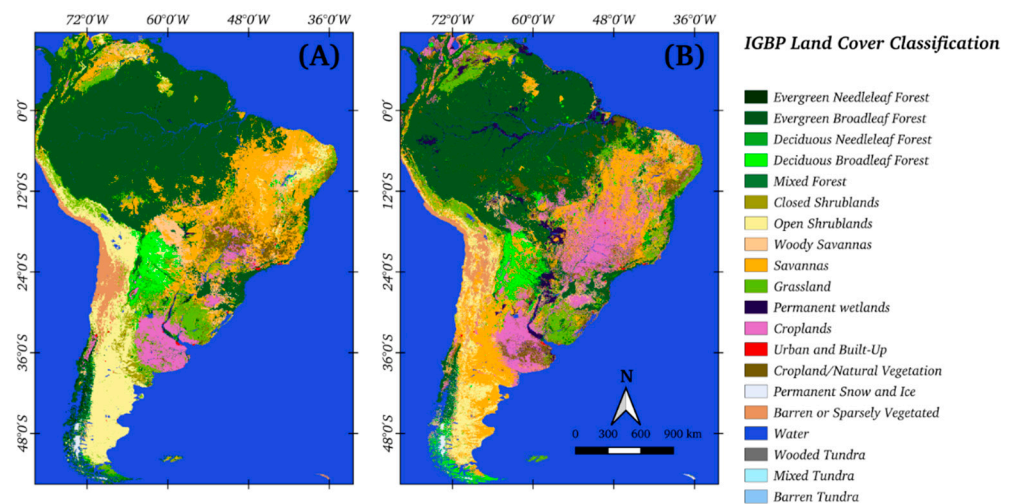


**Figure 5.** Land cover map for IGBP classification: (A) Noah-MP/WRF Standard LC; and (B) New Climatology ESACCI-LC 2010–2020.

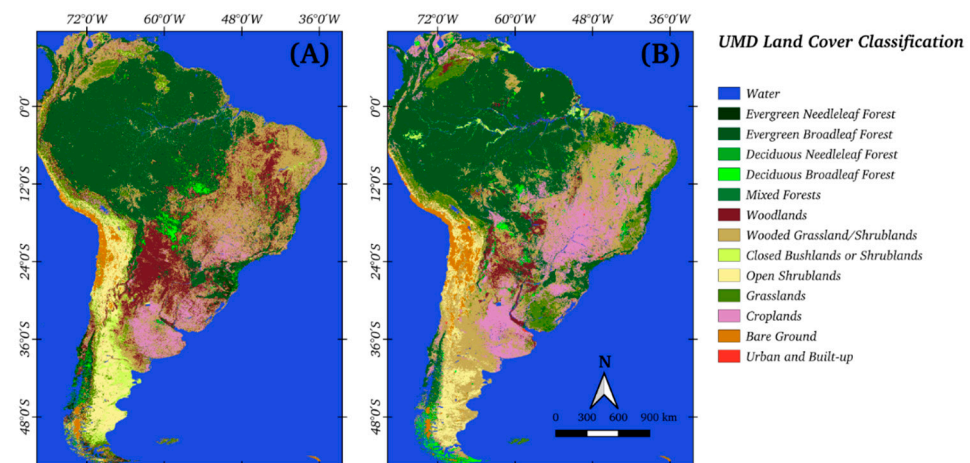


**Figure 6.** Land cover map for UMD classification: (A) CLSM Standard LC; and (B) New Climatology ESACCI-LC 2010–2020.

A comparison between the default land cover (LC) maps of the numerical models in SA, classified by the International Geosphere-Biosphere Programme (IGBP) and the University of Maryland (UMD), and the new LC maps based on the European Space Agency Climate Change Initiative (ESACCI) was conducted. The LC maps for the two Land Surface Model (LSM) classifications are illustrated in Figures 5 and 6.

Figure 5 displays LC maps for the IGBP LC classification, revealing notable changes between the two maps. The agriculture coverage area notably expands by approximately 1,270,661.90 km<sup>2</sup> (172.79%) compared to the initial area of 735,373 km<sup>2</sup>. This expansion is prominent in Brazil's central–southern and southeastern regions, the eastern part of northeastern Argentina, and a small area in the central region of Bolivia.

It is essential to highlight that the Agriculture/Natural Vegetation class also experiences a 122.02% expansion in its coverage area (Figure 5). Consequently, there is significant degradation in these highlighted areas, with a considerable expansion of agricultural areas leading to a reduction in natural areas across SA.

Figure 5 also shows the Bare Soil Vegetation class expansions over southwestern Bolivia. However, this class decreases in size in western Argentina and a small portion of the central region of Chile. The variation in the area of this class results in a reduction of approximately 9.53% (46,833.34 km<sup>2</sup>) compared to the initial area of 491,681 km<sup>2</sup>. It is worth noting that the region of the Salt Desert in Bolivia, initially classified as a water body, has been corrected to the Bare Soil class in the new LC. Other classes with significant coverage area variations include flooded areas, experiencing a 516.84% increase (150,110.51 km<sup>2</sup>) compared to the initial area of 29,044 km<sup>2</sup>. Closed Shrubland also sees growth of 218.0% (260,790.03 km<sup>2</sup>) compared to the initial area of 119,630 km<sup>2</sup> (Figure 5).

The new classification emphasizes flooded areas in the Brazilian Pantanal region, a known floodable area [51,52], and in the regions of the Amazon River and its tributaries, covering Brazil and Peru (Figure 5). These changes will directly impact surface flows, influencing the pattern of variation and affecting numerical simulations over the region.

In Figure 5, the Evergreen Needleleaf Forest and Wooded Tundra classes saw an over 85% reduction from their initial coverage areas—123,886 km<sup>2</sup> and 4595 km<sup>2</sup>, respectively. Conversely, the Mixed Forest, Wooded Savanna, and Permanent Snow and Ice classes exhibited approximately 75% variation compared to their initial areas—166,472 km<sup>2</sup>, 671,904 km<sup>2</sup>, and 24,833 km<sup>2</sup>—with only the Wooded Savanna class experiencing a reduction of about 515,000 km<sup>2</sup>.

The Open Shrubland class decreased by approximately 58% (1,207,393.43 km<sup>2</sup>). Simultaneously, the Deciduous Broadleaf Forest and Mixed Tundra classes saw reductions of 18.28% (85,342.65 km<sup>2</sup>) and 20.14% (37.29 km<sup>2</sup>), respectively. It is important to note that this LC update mapped the Evergreen Needleleaf Forest and Barren Tundra classes over SA. However, their coverage areas are less than 800 km<sup>2</sup>, making it challenging to identify on the map in Figure 5.

It is worth mentioning that the coverage classes, such as Evergreen Broadleaf Forest, Savannas, Pasture, and Urban and Built-up classes, had variations in coverage areas that were less than 6% of their initial areas. These areas were 7,623,213 km<sup>2</sup>, 2,828,317 km<sup>2</sup>, 1,594,027 km<sup>2</sup>, and 44,349 km<sup>2</sup>, respectively (Figure 5).

Figure 6 presents LC maps for the land cover UMD classification. Substantial differences between the maps are noted, with discrepancies in the classification of cover classes. It is relevant to highlight that the Urban and Built-up land cover class was not classified in the initial LC map, but was exclusively represented in the new LC product based on ESACCI. This class covers an area of approximately 52,397.42 km<sup>2</sup>.

Additionally, there is an apparent suppression of around 2,000,000 km<sup>2</sup> in the Woodlands coverage area. Replacements for this region includes cover classes such as Deciduous Broadleaf Forest, Croplands, and Wooded Grassland/Shrublands. The class showing the greatest expansion in area is Croplands, experiencing a growth of 128.0% (equivalent to 1,309,588.84 km<sup>2</sup>) compared to its original area of 1,022,691 km<sup>2</sup>. This expansion is observed in Brazil's central-western and Argentina's northeastern regions (Figure 6).

It is noteworthy to highlight that the expansion of Croplands primarily occurred over areas previously occupied by Wooded Grassland/Shrublands. In Brazil, this refers to the Cerrado biome, both the typical and sparse varieties [53,54]. In northeastern Argentina, this expansion is associated with the cover classes of Woodlands and Wooded Grassland/Shrublands [54,55].

The land cover classes that experienced the most significant suppression of their initial areas were Mixed Forest (−77.88%, equivalent to 68,026 km<sup>2</sup>) and Woodlands (−75.50%, equal to 2,034,272.4 km<sup>2</sup>). These classes mainly lost ground to the Croplands, Grassland, and Wooded Grassland/Shrublands cover classes [53,55,56].

### 3.3. New Vegetation Climatology

There is new climatological information for GVF and LAI in SA based on GLASS products [29,30,41]. Monthly maps of the updated climatology for these vegetation variables (GVF and LAI) from 2010 to 2020 over SA are presented in Figures 7 and 8. Figure 9 shows the monthly rainfall accumulations from the climatology of the MERGE product (2000–2022). In these figures, the seasonality of vegetation over SA and its response to changes in rainfall accumulations become evident. This pattern was expected as vegetation responds to water availability; when there is sufficient precipitation, vegetation exhibits greater vigor, resulting in improved plant health and increased leaf area [49,57].

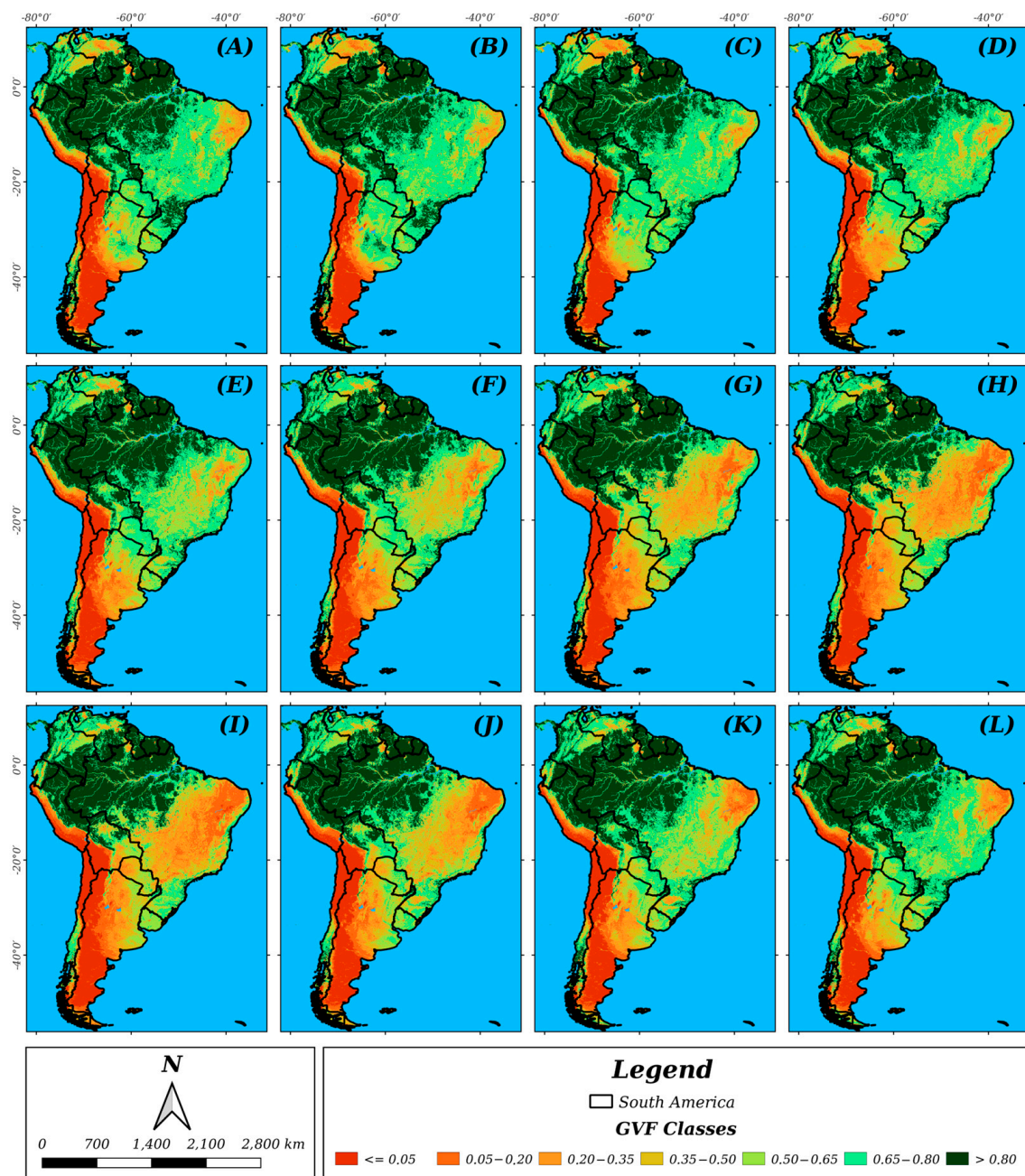


**Figure 7.** A spatial map of the monthly climatology for GVF over SA from 2010 to 2020 is shown, featuring the months of January (A); February (B); March (C); April (D); May (E); June (F); July (G); August (H); September (I); October (J); November (K); and December (L).

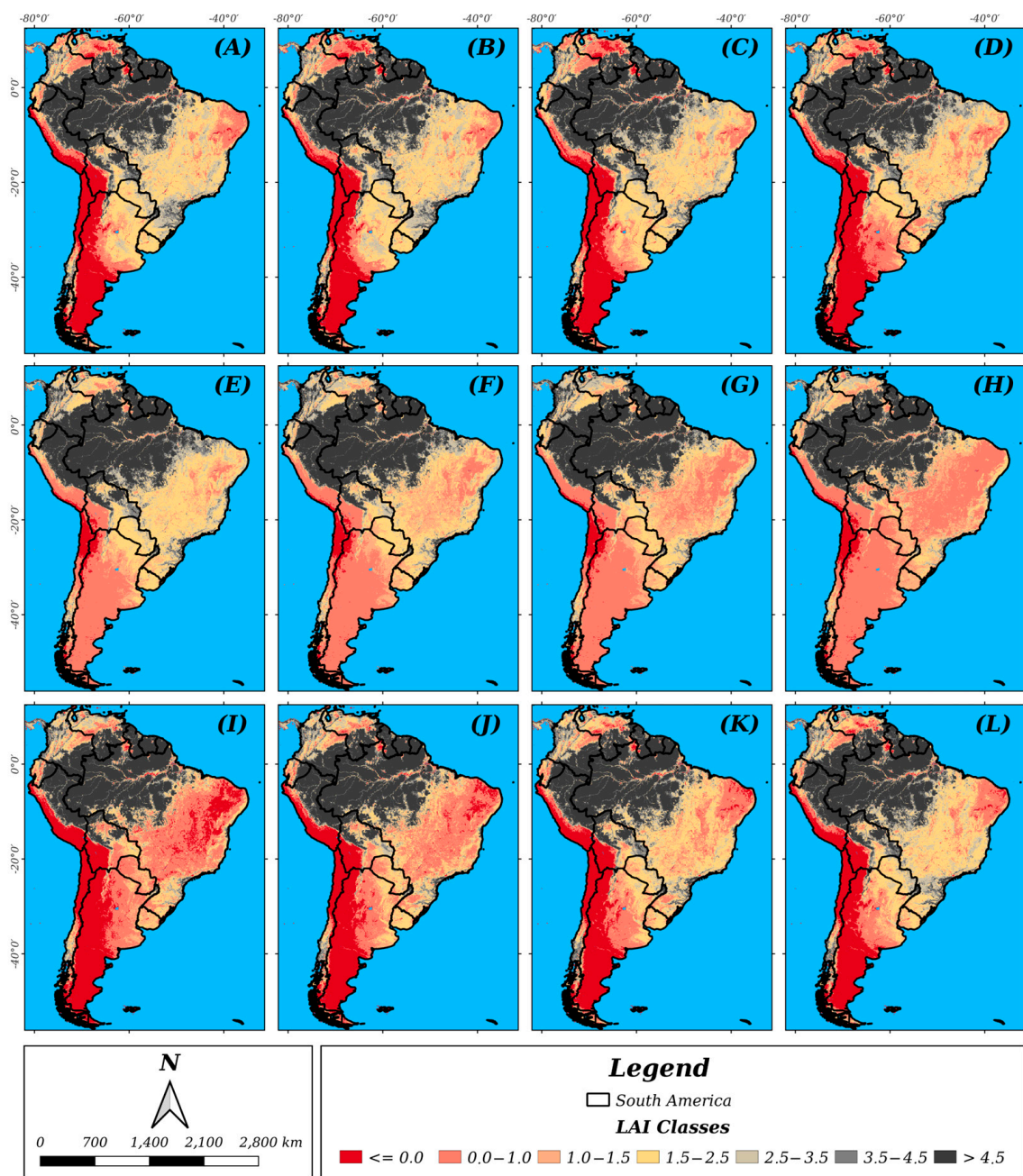


**Figure 8.** A spatial map of the monthly climatology for LAI over SA from 2010 to 2020 is shown, featuring the months of January (A); February (B); March (C); April (D); May (E); June (F); July (G); August (H); September (I); October (J); November (K); and December (L).

In Figures 7 and 8, the northeast and central–west regions of Brazil, Paraguay, southeastern Bolivia, and Argentina exhibit well-defined seasonality, with variation in the LAI and GVF values in response to periods of higher and lower rainfall accumulations, as illustrated in Figure 9. This pattern of vegetation variability was expected for these regions, as they are composed of biomes that respond rapidly to local rainfall. Among them, the Brazilian Cerrado and Caatinga stand out [2,49,57,58], and the Dry Chaco is present in Bolivia, Paraguay, and Argentina [23].

The coastal region of Brazil exhibits distinct GVF and LAI values compared to the more inland areas of the continent (Figures 7 and 8). This result is attributed to higher rainfall accumulations in this region (Figure 9), as moist winds from the ocean influence it

throughout the year. These winds significantly contribute to rainfall in the region [59–61]. The Amazon biome region, which covers Brazil, represents more than 60% of this Forest that encompasses Peru, Colombia, and Venezuela [62] and shows low variability in the GVF and LAI indices (Figures 7 and 8). In general, throughout the year, GVF values consistently exceed 0.80 (Figure 7), while LAI varies between  $3.5 \text{ m}^2/\text{m}^2$  and values greater than  $4.5 \text{ m}^2/\text{m}^2$  (Figure 9).

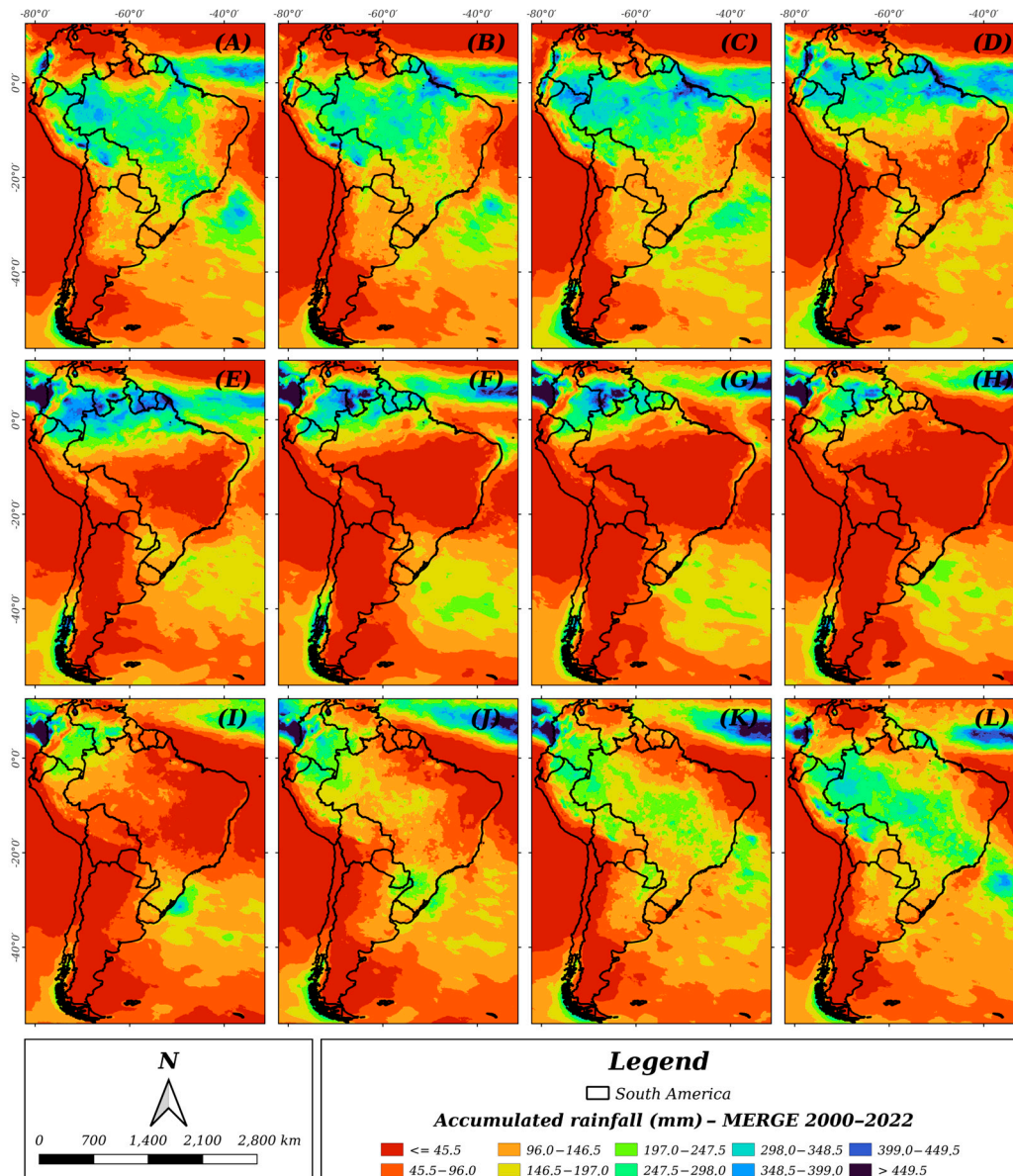


**Figure 9.** A spatial map of the monthly climatology of rainfall from the MERGE product for the period 2000–2022 over SA is presented, featuring the months of January (A); February (B); March (C); April (D); May (E); June (F); July (G); August (H); September (I); October (J); November (K); and December (L).

This region of the Amazon biome is characterized by high rainfall accumulations throughout the year, leading to the absence of a dry season [62,63] and maintaining rainfall occurrence throughout all months.

These high rainfall accumulations contribute to the low variability in vegetation indices in the Amazon rainforest. Additionally, the Forest plays a crucial role in maintaining the balance between climate and vegetation. The high evapotranspiration in the forest helps

sustain elevated rainfall accumulations throughout the region [62,64,65], thus supporting the local hydrological cycle.

Concerning the desert regions of SA, such as the Atacama Desert in Chile and the nearby arid areas, very low values of GVF and LAI are noticeable, with little variability throughout the months (Figures 7 and 8). For GVF, values are below 0.5 throughout the year, and for LAI, index values range between 0 and 1 m<sup>2</sup>/m<sup>2</sup>. Due to the arid nature of the region, rainfall accumulations are low throughout the year, not exceeding 45.5 mm/month (Figure 9).

In Figure 10, GVF scatter plots for land cover classes Cropland, Forest, Grass, and Savanna are presented, along with statistical indicators assessing input information from the MODIS numerical models for SA when compared to the new climatology based on GLASS (2010–2020).

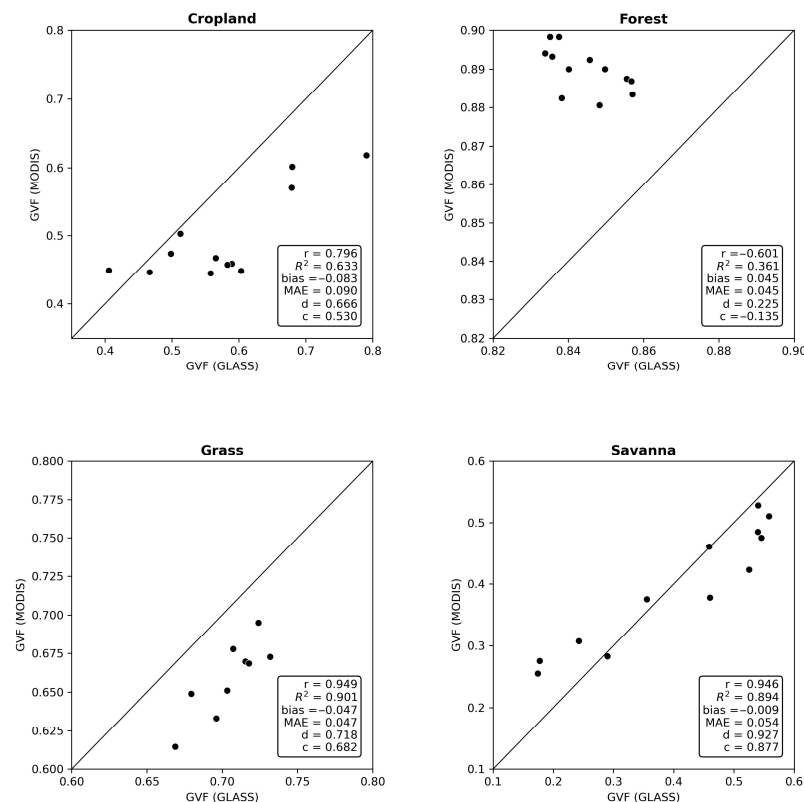


**Figure 10.** Statistical indicators for the standard GVF from numerical models in SA and the new monthly GVF climatology for 2010–2020 for different land cover classes.

It is observed that the Grass and Savanna classes exhibit a robust correlation ( $r > 0.9$ ), while the Cropland and Forest classes have correlations of 0.796 and 0.601, respectively. The coefficient of determination ( $R^2$ ) is low for the Forest class, moderate for Cropland, and high for both the Grass and Savanna classes, with  $R^2$  exceeding 0.85. The bias and MAE values for all land cover classes are also low. The highest (lowest) bias is for the Cropland class (Forest) with 0.083 (−0.009), while for MAE, the highest (lowest) is for the Cropland class (Forest) with 0.090 (0.045).

It is observed in Figure 10 that the agreement ‘d’ of the data is low for the Forest class, with a value below 0.5. For the Cropland and Grass classes, the ‘d’ index is moderate, ranging between 0.666 and 0.718, respectively. The ‘d’ index value for the Savanna class is high, exceeding 0.927, closer to unity, and better than the other highlighted classes.

Regarding the confidence index (c), a combination of ‘r’ and ‘d’ indices, it is noted that the Forest class shows a ‘Poor’ performance, with a ‘c’ value below 0 (Figure 10). The Cropland and Grass classes have a ‘Good’ performance, while the Savanna class has

an ‘Excellent’ performance. In this perspective, the Forest class requires updating of its representation in the numerical models for SA. In contrast, the Savanna class continues to be a good representation of the biome conditions. The Grass and Cropland classes still perform well, albeit lower than the Savanna class.

In Figure 11, LAI scatter plots for land cover classes Cropland, Forest, Grass, and Savanna are presented, along with statistical indicators to assess input information from the MODIS numerical models for SA when compared to the new climatology based on GLASS (2010–2020). It can be observed in Figure 11 that all land cover classes show a moderate correlation, ranging between 0.431 and 0.661. The  $R^2$  is low for all classes, with a value below 0.45. Additionally, bias and MAE values for all land cover classes are relatively high, representing an average of approximately 18.3% compared to the data medium. The highest error percentile is observed for the Cropland class (36.4%), followed by Savanna (21.0%), Grass (10.7%), and Forest (5.6%).

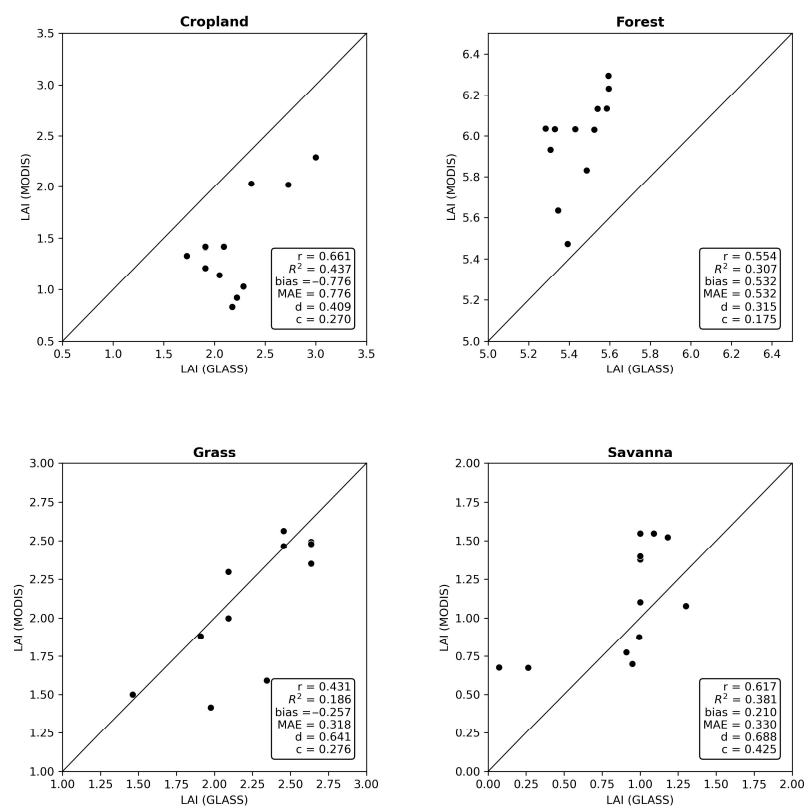


**Figure 11.** Statistical indicators for the standard LAI from numerical models in SA and the new monthly LAI climatology for the period 2010–2020 for different land cover classes.

Figure 11 shows that the agreement index (d) for Cropland and Forest classes is low, with values below 0.5. The d index is moderate for the Grass and Savanna classes, ranging between 0.641 and 0.688, respectively. Regarding the c index, all classes show ‘Poor’ or ‘Very Poor’ performance, with c values below 0.45. In this perspective, the need to update all LAI classes becomes evident, since the pattern of data variability is different. Thus, the default representation of MODIS in the numerical models of SA does not represent the region.

#### 4. Conclusions

In light of the investigations presented in this study, it becomes evident that significant changes have occurred in land cover and vegetation information over SA. These findings contribute to understanding regional landscape modifications and have important impli-



cations for numerical modeling. Therefore, generating new climatological information as input for these parameters is necessary.

The new climatological land cover maps indicated significant changes over SA, from expanding cropland areas exceeding 1 million km<sup>2</sup> to reducing native areas by around 500 thousand km<sup>2</sup>. Furthermore, the new land cover climatology demonstrates remarkable performance in representing cover classes, with an overall accuracy exceeding 80% for both the IGBP (89.83%) and UMD (80.03%) classifications. Thus, these new land cover climatologies are excellent options for initializing numerical models in the region, being more recent and accurately representing the current surface conditions of SA.

Despite achieving an accuracy above 80%, the new mapping still holds uncertainties, particularly in complex landscapes. Future research should concentrate on refining land cover mapping accuracy. This goal can be accomplished by utilizing advanced techniques in remote sensing and integrating high-resolution satellite data for more detailed analysis.

Regarding vegetation information, it is concluded that updating climatic GVF and LAI maps is necessary due to changes in land cover, which directly impact these indices. New GVF and LAI climatology maps were developed in this context, revealing distinct temporal patterns compared to the standard information from South America's numerical models.

Statistical indicators highlighted this information, indicating a low correlation, a low agreement between series, and a c index performance classified as "Poor" or "Very Poor", especially for the LAI index. On the other hand, the GVF index shows better performance, where the c index performance is "Good" and "Excellent" for Cropland, Grass, and Savanna classes. In contrast, the Forest class exhibited a "Very Poor" performance.

Considering the challenges identified in the statistical indicators of LAI and GVF indices with changes in land cover, future studies can deepen the understanding of factors influencing these discrepancies. To achieve our goal, we need to conduct thorough field validations, incorporate more environmental variables, and improve our modeling techniques.

In conclusion, while this study provides a comprehensive assessment of changes in land cover and vegetation in South America, ongoing research is needed to address identified limitations and advance our understanding of regional dynamics. Future studies could benefit from a multidisciplinary approach, incorporating advanced technologies and refining methodologies to enhance the accuracy and reliability of climatological information and its application in numerical models.

**Author Contributions:** Conceptualization, L.E.R.A. and L.G.G.d.G.; methodology, L.E.R.A. and L.G.G.d.G.; software, L.E.R.A.; validation, L.E.R.A., G.C.d.N. and W.L.F.C.F.; formal analysis, L.E.R.A., B.B.M., Á.V.A.d.Á., W.L.F.C.F. and G.D.G.; investigation, L.E.R.A., B.B.M., Á.V.A.d.Á. and G.D.G.; resources, G.C.d.N. and L.G.G.d.G.; data curation, L.E.R.A.; writing—original draft preparation, L.E.R.A.; writing—review and editing, L.G.G.d.G., B.B.M., Á.V.A.d.Á., G.D.G., G.C.d.N. and W.L.F.C.F.; visualization, L.E.R.A.; supervision, L.G.G.d.G.; funding acquisition, L.E.R.A. and L.G.G.d.G. All authors have read and agreed to the published version of the manuscript.

**Funding:** The authors thank the Coordination for the Improvement of Higher Education Personnel (CAPES–Brasil, funding code 001) for financial support.

**Institutional Review Board Statement:** Not applicable.

**Informed Consent Statement:** Not applicable.

**Data Availability Statement:** Data are contained within the article.

**Acknowledgments:** The authors are grateful for the computational and financial support provided by the Center for Weather Forecasting and Climate Studies of the National Institute for Space Research (CPTEC/INPE). And the first author would like to thank the Coordination for the Improvement of Higher Education Personnel (CAPES) for granting a doctoral scholarship. And also thank you for support from the IAEA CRP on "Enhancing Agricultural Resilience and Water Security Using Cosmic-Ray Neutron Sensor" (D12014).

**Conflicts of Interest:** The authors declare no conflicts of interest.

## References

1. Poulter, B.; MacBean, N.; Hartley, A.; Khlystova, I.; Arino, O.; Betts, R.; Bontemps, S.; Boettcher, M.; Brockmann, C.; Defourny, P.; et al. Plant Functional Type Classification for Earth System Models: Results from the European Space Agency's Land Cover Climate Change Initiative. *Geosci. Model Dev.* **2015**, *8*, 2315–2328. [[CrossRef](#)]
2. Salazar, A.; Baldi, G.; Hirota, M.; Syktus, J.; McAlpine, C. Land Use and Land Cover Change Impacts on the Regional Climate of Non-Amazonian South America: A Review. *Glob. Planet. Chang.* **2015**, *128*, 103–119. [[CrossRef](#)]
3. Silva, M.E.S.; Pereira, G.; da Rocha, R.P. Local and Remote Climatic Impacts Due to Land Use Degradation in the Amazon "Arc of Deforestation". *Theor. Appl. Climatol.* **2016**, *125*, 609–623. [[CrossRef](#)]
4. Oliveira, L.N.; de Aquino, C.M.S. Dinâmica temporal do uso e cobertura da terra na fronteira agrícola do matopiba: Análise na sub-bacia hidrográfica do rio Gurguéia-Piauí. *Rev. Equador* **2020**, *9*, 317–333. [[CrossRef](#)]
5. Schneider, M.; Biedzicki de Marques, A.A.; Peres, C.A. Brazil's Next Deforestation Frontiers. *Trop. Conserv. Sci.* **2021**, *14*, 19400829211020472. [[CrossRef](#)]
6. Brando, P.; Macedo, M.; Silvério, D.; Rattis, L.; Paolucci, L.; Alencar, A.; Coe, M.; Amorim, C. Amazon Wildfires: Scenes from a Foreseeable Disaster. *Flora* **2020**, *268*, 151609. [[CrossRef](#)]
7. Song, X.-P.; Hansen, M.C.; Potapov, P.; Adusei, B.; Pickering, J.; Adami, M.; Lima, A.; Zalles, V.; Stehman, S.V.; Di Bella, C.M.; et al. Massive Soybean Expansion in South America since 2000 and Implications for Conservation. *Nat. Sustain.* **2021**, *4*, 784–792. [[CrossRef](#)]
8. Zalles, V.; Hansen, M.C.; Potapov, P.V.; Parker, D.; Stehman, S.V.; Pickens, A.H.; Parente, L.L.; Ferreira, L.G.; Song, X.-P.; Hernandez-Serna, A.; et al. Rapid Expansion of Human Impact on Natural Land in South America since 1985. *Sci. Adv.* **2021**, *7*, eabg1620. [[CrossRef](#)]
9. Rodell, M.; Houser, P.R.; Jambor, U.; Gottschalck, J.; Mitchell, K.; Meng, C.-J.; Arsenault, K.; Cosgrove, B.; Radakovich, J.; Bosilovich, M.; et al. The Global Land Data Assimilation System. *Bull. Am. Meteorol. Soc.* **2004**, *85*, 381–394. [[CrossRef](#)]
10. De Goncalves, L.G.G.; Shuttleworth, W.J.; Burke, E.J.; Houser, P.; Toll, D.L.; Rodell, M.; Arsenault, K. Toward a South America Land Data Assimilation System: Aspects of Land Surface Model Spin-up Using the Simplified Simple Biosphere. *J. Geophys. Res. Atmos.* **2006**, *111*, D17110. [[CrossRef](#)]
11. de Ávila, Á.V.A.; de Gonçalves, L.G.G.; Souza, V.d.A.; Alves, L.E.R.; Galetti, G.D.; Maske, B.M.; Getirana, A.; Ruhoff, A.; Biudes, M.S.; Machado, N.G.; et al. Assessing the Performance of the South American Land Data Assimilation System Version 2 (SALDAS-2) Energy Balance across Diverse Biomes. *Atmosphere* **2023**, *14*, 959. [[CrossRef](#)]
12. Zhen, Z.; Chen, S.; Yin, T.; Chavanon, E.; Laurent, N.; Guilleux, J.; Henke, M.; Qin, W.; Cao, L.; Li, J.; et al. Using the negative soil adjustment factor of soil adjusted vegetation index (SAVI) to resist saturation effects and estimate leaf area index (lai) in dense vegetation areas. *Sensors* **2021**, *21*, 2115. [[CrossRef](#)]
13. Filipponi, F.; Valentini, E.; Xuan, A.N.; Guerra, C.A.; Wolf, F.; Andrzejak, M.; Taramelli, A. Global MODIS Fraction of Green Vegetation Cover for Monitoring Abrupt and Gradual Vegetation Changes. *Remote Sens.* **2018**, *10*, 653. [[CrossRef](#)]
14. Pilotto, I.L.; Rodríguez, D.A.; Chan Chou, S.; Tomasella, J.; Sampaio, G.; Gomes, J.L. Effects of the Surface Heterogeneities on the Local Climate of a Fragmented Landscape in Amazonia Using a Tile Approach in the Eta/Noah-MP Model. *Q. J. R. Meteorol. Soc.* **2017**, *143*, 1565–1580. [[CrossRef](#)]
15. Toure, A.M.; Reichle, R.H.; Forman, B.A.; Getirana, A.; De Lannoy, G.J.M. Assimilation of MODIS Snow Cover Fraction Observations into the NASA Catchment Land Surface Model. *Remote Sens.* **2018**, *10*, 316. [[CrossRef](#)]
16. Fernandez, J.P.R.; Figueroa, S.N.; Éder, P.V.; Herdies, D.L.; Gonçalves, L.G.G.; Aravéquia, J.A. *Relatório de Avaliação do Modelo CPT-WRF v1.2*; Instituto Nacional de Pesquisas Espaciais: Cachoeira Paulista, Brazil, 2021; pp. 1–30.
17. Bonan, G.B.; Levis, S.; Kergoat, L.; Oleson, K.W. Landscapes as Patches of Plant Functional Types: An Integrating Concept for Climate and Ecosystem Models. *Glob. Biogeochem. Cycles* **2002**, *16*, 5-1–5-23. [[CrossRef](#)]
18. Kumar, S.V.; Peters-Lidard, C.D.; Tian, Y.; Houser, P.R.; Geiger, J.; Olden, S.; Lighty, L.; Eastman, J.L.; Doty, B.; Dirmeyer, P.; et al. Land Information System: An Interoperable Framework for High Resolution Land Surface Modeling. *Environ. Model. Softw.* **2006**, *21*, 1402–1415. [[CrossRef](#)]
19. Chen, L.; Ma, Z.; Zhao, T. Modeling and Analysis of the Potential Impacts on Regional Climate Due to Vegetation Degradation over Arid and Semi-Arid Regions of China. *Clim. Chang.* **2017**, *144*, 461–473. [[CrossRef](#)]
20. Lee, S.-J.; Berbery, E.H. Land Cover Change Effects on the Climate of the La Plata Basin. *J. Hydrometeorol.* **2012**, *13*, 84–102. [[CrossRef](#)]
21. Fang, L.; Zhan, X.; Hain, C.R.; Liu, J. Impact of Using Near Real-Time Green Vegetation Fraction in Noah Land Surface Model of NOAA NCEP on Numerical Weather Predictions. *Adv. Meteorol.* **2018**, *2018*, 9256396. [[CrossRef](#)]
22. Kumar, S.V.; Mocko, D.M.; Wang, S.; Peters-Lidard, C.D.; Borak, J. Assimilation of Remotely Sensed Leaf Area Index into the Noah-MP Land Surface Model: Impacts on Water and Carbon Fluxes and States over the Continental United States. *J. Hydrometeorol.* **2019**, *20*, 1359–1377. [[CrossRef](#)]
23. Maertens, M.; De Lannoy, G.J.M.; Apers, S.; Kumar, S.V.; Mahanama, S.P.P. Land Surface Modeling over the Dry Chaco: The Impact of Model Structures, and Soil, Vegetation and Land Cover Parameters. *Hydrol. Earth Syst. Sci.* **2021**, *25*, 4099–4125. [[CrossRef](#)]

24. Wang, X.; Zhang, Z.; Zhang, B.; Tian, L.; Arnault, J.; Kunstmann, H.; He, C. Quantifying the Impact of Land Use and Land Cover Change on Moisture Recycling with Convective-Permitting WRF-Tagging Modeling in the Agro-Pastoral Ecotone of Northern China. *J. Geophys. Res. Atmos.* **2023**, *128*, e2022JD038421. [[CrossRef](#)]
25. Guo, Z.; Ferrer, J.V.; Hürlimann, M.; Medina, V.; Puig-Polo, C.; Yin, K.; Huang, D. Shallow landslide susceptibility assessment under future climate and land cover changes: A case study from southwest China. *Geosci. Front.* **2023**, *14*, 101542. [[CrossRef](#)]
26. Zhang, Q.; Sun, Q.; Dai, G.; Mu, M. Impact of Uncertainties in Land Surface Processes on Subseasonal Predictability of Heat Waves Onset Over the Yangtze River Valley. *J. Geophys. Res. Atmos.* **2024**, *129*, e2023JD038674. [[CrossRef](#)]
27. Barati, A.A.; Zhooldideh, M.; Azadi, H.; Lee, J.; Scheffran, J. Interactions of Land-Use Cover and Climate Change at Global Level: How to Mitigate the Environmental Risks and Warming Effects. *Ecol. Indic.* **2023**, *146*, 109829. [[CrossRef](#)]
28. Giri, C.; Long, J. Land Cover Characterization and Mapping of South America for the Year 2010 Using Landsat 30 m Satellite Data. *Remote Sens.* **2014**, *6*, 9494–9510. [[CrossRef](#)]
29. Xiao, Z.; Liang, S.; Wang, J.; Chen, P.; Yin, X.; Zhang, L.; Song, J. Use of General Regression Neural Networks for Generating the GLASS Leaf Area Index Product from Time-Series MODIS Surface Reflectance. *IEEE Trans. Geosci. Remote Sens.* **2014**, *52*, 209–223. [[CrossRef](#)]
30. Jia, K.; Liang, S.; Wei, X.; Yao, Y.; Yang, L.; Zhang, X.; Liu, D. Validation of Global Land Surface Satellite (GLASS) Fractional Vegetation Cover Product from MODIS Data in an Agricultural Region. *Remote Sens. Lett.* **2018**, *9*, 847–856. [[CrossRef](#)]
31. Xu, B.; Li, J.; Park, T.; Liu, Q.; Zeng, Y.; Yin, G.; Zhao, J.; Fan, W.; Yang, L.; Knyazikhin, Y.; et al. An Integrated Method for Validating Long-Term Leaf Area Index Products Using Global Networks of Site-Based Measurements. *Remote Sens. Environ.* **2018**, *209*, 134–151. [[CrossRef](#)]
32. Copernicus Climate Change Service, Climate Data Store. Land Cover Classification Gridded Maps from 1992 to Present Derived from Satellite Observations. Copernicus Climate Change Service (C3S) Climate Data Store (CDS). [[CrossRef](#)]
33. Buchhorn, M.; Lesiv, M.; Tsendbazar, N.-E.; Herold, M.; Bertels, L.; Smets, B. Copernicus Global Land Cover Layers—Collection 2. *Remote Sens.* **2020**, *12*, 1044. [[CrossRef](#)]
34. Broxton, P.D.; Zeng, X.; Sulla-Menashe, D.; Troch, P.A. A Global Land Cover Climatology Using MODIS Data. *J. Appl. Meteorol. Climatol.* **2014**, *53*, 1593–1605. [[CrossRef](#)]
35. Hansen, M.C.; Defries, R.S.; Townshend, J.R.G.; Sohlberg, R. Global Land Cover Classification at 1 Km Spatial Resolution Using a Classification Tree Approach. *Int. J. Remote Sens.* **2000**, *21*, 1331–1364. [[CrossRef](#)]
36. Llano, X.C. AcATaMa—QGIS Python Plugins Repository. Available online: <https://plugins.qgis.org/plugins/AcATaMa/> (accessed on 30 December 2023).
37. Novo, E.M.L.d.M. *Sensoriamento Remoto: Princípios e Aplicações*, 4th ed.; Blucher: São Paulo, Brazil, 2010; ISBN 978-85-212-0540-1.
38. Olofsson, P.; Foody, G.M.; Stehman, S.V.; Woodcock, C.E. Making Better Use of Accuracy Data in Land Change Studies: Estimating Accuracy and Area and Quantifying Uncertainty Using Stratified Estimation. *Remote Sens. Environ.* **2013**, *129*, 122–131. [[CrossRef](#)]
39. Olofsson, P.; Foody, G.M.; Herold, M.; Stehman, S.V.; Woodcock, C.E.; Wulder, M.A. Good Practices for Estimating Area and Assessing Accuracy of Land Change. *Remote Sens. Environ.* **2014**, *148*, 42–57. [[CrossRef](#)]
40. Xiao, Z.; Liang, S.; Wang, J.; Xiang, Y.; Zhao, X.; Song, J. Long-Time-Series Global Land Surface Satellite Leaf Area Index Product Derived from MODIS and AVHRR Surface Reflectance. *IEEE Trans. Geosci. Remote Sens.* **2016**, *54*, 5301–5318. [[CrossRef](#)]
41. Jia, K.; Yang, L.; Liang, S.; Xiao, Z.; Zhao, X.; Yao, Y.; Zhang, X.; Jiang, B.; Liu, D. Long-Term Global Land Surface Satellite (GLASS) Fractional Vegetation Cover Product Derived from MODIS and AVHRR Data. *IEEE J. Sel. Top. Appl. Earth Obs. Remote Sens.* **2019**, *12*, 508–518. [[CrossRef](#)]
42. Kaufmann, R.K.; Zhou, L.; Knyazikhin, Y.; Shabanov, V.; Myneni, R.B.; Tucker, C.J. Effect of Orbital Drift and Sensor Changes on the Time Series of AVHRR Vegetation Index Data. *IEEE Trans. Geosci. Remote Sens.* **2000**, *38*, 2584–2597. [[CrossRef](#)]
43. Gutman, G.; Ignatov, A. The Derivation of the Green Vegetation Fraction from NOAA/AVHRR Data for Use in Numerical Weather Prediction Models. *Int. J. Remote Sens.* **1998**, *19*, 1533–1543. [[CrossRef](#)]
44. Camargo, A.P.; Sentelhas, P.C. Avaliação do desempenho de diferentes métodos de estimativa da evapotranspiração potencial no estado de São Paulo, Brasil. *Rev. Bras. Agrometeorol.* **1997**, *5*, 89–97.
45. Pereira, D.d.R.; Yanagi, S.d.N.M.; de Mello, C.R.; da Silva, A.M.; da Silva, L.A. Desempenho de métodos de estimativa da evapotranspiração de referência para a região da Serra da Mantiqueira, MG. *Ciênc. Rural* **2009**, *39*, 2488–2493. [[CrossRef](#)]
46. Moreira, T.d.J.R.V.; dos Santos, M.R.; Moreira, A.L. *Estatística Básica*, 1st ed.; EdUESPI: Teresina, PI, Brazil, 2021.
47. Rozante, J.R.; Gutierrez, E.R.; Fernandes, A.D.A.; Vila, D.A. Performance of Precipitation Products Obtained from Combinations of Satellite and Surface Observations. *Int. J. Remote Sens.* **2020**, *41*, 7585–7604. [[CrossRef](#)]
48. Righi, C.A.; Risante, A.P.O.; Packer, A.P.; Couto, H.T.Z. Biodiversity and biomass relationships in a Cerrado Stricto sensu in Southeastern Brazil. *Environ. Monit. Assess.* **2023**, *195*, 492. [[CrossRef](#)]
49. Dos Santos, F.S.; Gomes, H.B.; de Barros, G.V.P.; Alves, L.E.R.; da Silva, D.F.; Costa, R.L.; Silva, F.D.d.S.; de Oliveira, J.F. Análise Sazonal dos Parâmetros Biofísicos Utilizando o Sensor MODIS para o Estado de Alagoas. *Rev. Bras. Meteorol.* **2021**, *35*, 955–968. [[CrossRef](#)]
50. Zimbres, B.; Rodríguez-Veiga, P.; Shimbo, J.Z.; Bispo, P.C.; Balzter, H.; Bustamante, M.; Roitman, I.; Haidar, R.; Miranda, S.; Gomes, L.; et al. Mapping the stock and spatial distribution of aboveground woody biomass in the native vegetation of the Brazilian Cerrado biome. *For. Ecol. Manag.* **2021**, *499*, 119615. [[CrossRef](#)]

51. Goltz, E.; Brandão, D.; Tomás, L.; Mantelli, L.R.; Adami, M.; Shimabukuro, Y.E.; Formaggio, A.R. Utilização de índices espectrais de vegetação do sensor MODIS na determinação de áreas suscetíveis a alagamento no pantanal sulmatogrossense/Use of MODIS Spectral Vegetation Indices to Determine Susceptible Flooding Area in the Pantanal Sulmatogrossense. *Rev. Bras. Cartogr.* **2007**, *59*, 35–44.
52. Vourlitis, G.L.; Pinto, O.B.; Dalmagro, H.J.; de Arruda, P.E.Z.; de Almeida Lobo, F.; de Souza Nogueira, J. Tree Growth Responses to Climate Variation in Upland and Seasonally Flooded Forests and Woodlands of the Cerrado-Pantanal Transition of Brazil. *For. Ecol. Manag.* **2022**, *505*, 119917. [[CrossRef](#)]
53. Noojipady, P.; Morton, C.D.; Macedo, N.M.; Victoria, C.D.; Huang, C.; Gibbs, K.H.; Bolfe, L.E. Forest Carbon Emissions from Cropland Expansion in the Brazilian Cerrado Biome. *Environ. Res. Lett.* **2017**, *12*, 025004. [[CrossRef](#)]
54. De Espindola, G.M.; Figueredo, E.d.S.; Júnior, P.P.; Filho, A.A.d.R. Cropland Expansion as a Driver of Land-Use Change: The Case of Cerrado-Caatinga Transition Zone in Brazil. *Environ. Dev. Sustain.* **2021**, *23*, 17146–17160. [[CrossRef](#)]
55. Stanimirova, R.; Graesser, J.; Olofsson, P.; Friedl, M.A. Widespread Changes in 21st Century Vegetation Cover in Argentina, Paraguay, and Uruguay. *Remote Sens. Environ.* **2022**, *282*, 113277. [[CrossRef](#)]
56. Piquer-Rodríguez, M.; Butsic, V.; Gärtner, P.; Macchi, L.; Baumann, M.; Gavier Pizarro, G.; Volante, J.N.; Gasparri, I.N.; Kuemmerle, T. Drivers of Agricultural Land-Use Change in the Argentine Pampas and Chaco Regions. *Appl. Geogr.* **2018**, *91*, 111–122. [[CrossRef](#)]
57. Alves, L.E.R.; Gomes, H.B.; dos Santos, F.S.; Correia Filho, W.L.F.; de Oliveira Júnior, J.F. Parâmetros Biofísicos Aplicados no Parque Nacional da Serra das Confusões, Piauí-Brasil. *Rev. Bras. Meteorol.* **2020**, *35*, 597–604. [[CrossRef](#)]
58. Silva, B.K.N.; Amorim, A.C.B.; Silva, C.M.S.; Lucio, P.S.; Barbosa, L.M. Rainfall-Related Natural Disasters in the Northeast of Brazil as a Response to Ocean-Atmosphere Interaction. *Theor. Appl. Climatol.* **2019**, *138*, 1821–1829. [[CrossRef](#)]
59. Correia Filho, W.L.F.; De Oliveira-Júnior, J.F.; De Barros Santiago, D.; De Bodas Terassi, P.M.; Teodoro, P.E.; De Gois, G.; Blanco, C.J.C.; De Almeida Souza, P.H.; da Silva Costa, M.; Gomes, H.B.; et al. Rainfall Variability in the Brazilian Northeast Biomes and Their Interactions with Meteorological Systems and ENSO via CHELSA Product. *Big Earth Data* **2019**, *3*, 315–337. [[CrossRef](#)]
60. De Oliveira-Júnior, J.F.; Correia Filho, W.L.F.; de Barros Santiago, D.; de Gois, G.; da Silva Costa, M.; da Silva Junior, C.A.; Teodoro, P.E.; Freire, F.M. Rainfall in Brazilian Northeast via in Situ Data and CHELSA Product: Mapping, Trends, and Socio-Environmental Implications. *Environ. Monit. Assess.* **2021**, *193*, 263. [[CrossRef](#)]
61. Silva, A.S.D.; Silva, E.M.D.; Leal Junior, J.B.V.; Sales, D.C.; Moura, I.J.M.; Alves, J.M.B. Distúrbios Ondulatórios de Leste no Nordeste Brasileiro: Um Estudo de Caso Utilizando Modelagem Numérica de Mesoescala. *Rev. Bras. Meteorol.* **2021**, *36*, 637–649. [[CrossRef](#)]
62. Marengo, J.A.; Tomasella, J.; Alves, L.M.; Soares, W.R.; Rodriguez, D.A. The Drought of 2010 in the Context of Historical Droughts in the Amazon Region. *Geophys. Res. Lett.* **2011**, *38*, L12703. [[CrossRef](#)]
63. Dos Santos, T.O.; Filho, V.S.d.A.; França, R.d.S. Variabilidade e tendência climática nos municípios de Manaus (AM) e São Gabriel da Cachoeira (AM): Uma avaliação a partir dos dados de precipitação e temperatura. *Rev. Geonorte* **2023**, *14*, 149–171. [[CrossRef](#)]
64. Kunert, N.; Aparecido, L.M.T.; Wolff, S.; Higuchi, N.; dos Santos, J.; de Araujo, A.C.; Trumbore, S. A Revised Hydrological Model for the Central Amazon: The Importance of Emergent Canopy Trees in the Forest Water Budget. *Agric. For. Meteorol.* **2017**, *239*, 47–57. [[CrossRef](#)]
65. Baker, J.C.A.; Garcia-Carreras, L.; Gloor, M.; Marsham, J.H.; Buermann, W.; da Rocha, H.R.; Nobre, A.D.; de Araujo, A.C.; Spracklen, D.V. Evapotranspiration in the Amazon: Spatial Patterns, Seasonality, and Recent Trends in Observations, Reanalysis, and Climate Models. *Hydrol. Earth Syst. Sci.* **2021**, *25*, 2279–2300. [[CrossRef](#)]

**Disclaimer/Publisher’s Note:** The statements, opinions and data contained in all publications are solely those of the individual author(s) and contributor(s) and not of MDPI and/or the editor(s). MDPI and/or the editor(s) disclaim responsibility for any injury to people or property resulting from any ideas, methods, instructions or products referred to in the content.